Object Handover between Humans and Robots in Microgravity

Adriana Maria Marques Fernandes
adrianafernandes@tecnico.ulisboa.pt

Instituto Superior Técnico, Lisboa, Portugal

February 2020

Abstract

The collaborative space robots field is an emerging research field with high impact as robots perform collaborative missions with high precision during lengthy tasks, on an accelerated schedule and do not require spacial suits, infrastructures such as life support or to return to Earth, making them efficient and economically viable. However, human-robot collaboration in space is still a challenge concerning key issues such as manipulation of weightless objects and mobility due to the peculiar motion dynamics of the robot and the manipulator on a microgravity environment. Therefore, this dissertation aims to formulate an algorithm that enables a free-flyer robot equipped with a manipulator to perform a successful, fluent and dynamic robot-to-human and human-to-robot object handover. Additionally, a systematic user study is proposed with the goal of analysing the user's preferences between a rigid and compliant impedance robot behavior during the object handover and understanding the impact of those behaviors on the success of the task. The proposed algorithm is formulated with resource to a finite-state machine that encompasses a designed impedance controller for the transfer phase enabling a dynamic interaction between both task participants. Following, the algorithm is implemented and validated on the simulator of NASA's Astrobee free-flyer robot and the two impedance behaviors, rigid and compliant, are successfully studied. Furthermore, an user interaction interface is developed and includes an user simulated hand model controlled via a Leap Motion device. This interface generates a virtual reality perception environment that enables an accurate interaction with the robot on the proposed tasks. Lastly, the proposed systematic user study was conducted. Results showed that the rigid behavior was overall more preferable and registered higher transfer success during the tasks.

Keywords: Human-Robot Collaboration, Microgravity Object Handover, Space Manipulation, Force Control, Impedance Control, Virtual Reality

1. Introduction

The field of space research encompasses distinct research branches such as earth observation, solar and space physics concerning primarily with electromagnetic effects, cosmology and research on nonliving and living materials such as humans and robots in microgravity. This dissertation focus on the last field, more specifically, on the collaborative space robotics field. Collaborative space robotics research is considered the development of general purpose machines that are able to operate in microgravity environments facilitating manipulation, assembling or servicing functions in collaboration with astronauts. One of the reasons why space robots became progressively more relevant to the current overall ability to operate in space is their capability to function for longer periods without the need of interrupting the task, in contrast to humans due to their essential needs. Furthermore, robots are able to replicate flawlessly the same task and on an accelerated schedule. Robots also operate with extreme high precision which is crucial on a demanding and rigorous research environment such as space. Additionally, outstaying advantages of space robots concern about the decrease of risk compared to human life and robot's impassibility towards the low temperatures, not needing long pre-arrangements or expensive suits before going to outer space. Moreover, another cost associated with humans and not with robots is the need to return to Earth. The replacement of NASA's crew on board of SpaceX Dragon or Boeing CST-100 cost 56 millions per seat, in 2016[1]. In this manner, access to space is expensive implying that robots are economically attractive for a broad classes of missions. Additionally, it is relevant to refer key issues concerning space robots such as manipulation and mobility. Although this issues are a basic technology in robotics, microgravity in the orbital environment requires further attention

[1]NASA (2016). Commercial Crew Transportation Program, Retrieved November 5, 2019, from https://www.nasa.gov/sites/default/files/atoms/files.

due to the peculiar motion dynamics of the robot and manipulator, especially in collaborative tasks with humans such as object handovers.

Given the advantages of space robotics, the goal of the dissertation is to formulate an algorithm that enables a free-flyer robot equipped with a manipulator to perform an object handover with a human on a successful, fluent and dynamic manner in a microgravity environment. Furthermore, this thesis aims to conduct a systematic user study with the goal of understanding the subjective outcome effects of a rigid and compliant impedance robot behavior during the interaction. Additionally, the study intends to analyse the impact of those behaviors on the success of the task. To encounter with the proposed goals, a Finite State Machine (FSM) is formulated for a robot-to-human and human-to-robot object handover in which an impedance control approach is designed for the transfer phase and two distinct robot impedance behaviors are studied: rigid and compliant. Moreover, an user interaction interface is implemented and it aims to deliver a virtual reality experience for the user.

This extended abstract is structured as follows: the State-of-the-art is explored in Section 2, the Handover Algorithm Formulation is described in Section 3, including the derivation of the impedance controller. Furthermore, the Implementation and Results are presented in Section 4, the User Study is shown in Section 5 and Section 6 includes concluding remarks with future work references.

2. State-of-the-Art

Many advances were made regarding collaborative space robotics challenges but, to the best of the authors knowledge, no record on the field of object handover between humans and robots in microgravity was found in the literature. Nevertheless, it is important to state relevant research in terrestrial object handovers of each of the phases: approach, transfer and retraction. Regarding the first phase, Cakmak in [1] showed that robot's postures with an extended arm were most frequently classified handing over and Koay in [10] concluded that the robot should approach the user from the front. Furthermore, Aleotti in [9] stated that robots should take into consideration how the human will grasp the object and thus robots should approach the user with the easiest part to grasp of the object. Regarding the transfer phase, Edsinger in [3] found that humans will pose an object in the robot's stationary hand regardless of the robot's hand pose. Regarding the communication intent, Strabala in [14] claims that special signals can be used when the human and robot share the meaning of these signals in a common ground. Concerning the decision of releasing or grasping an object, Edsinger in [3] monitored the velocity of the robot's end-effector. To achieve a dynamic handover, Kupcsik's studied a Cartesian impedance control approach [12] and Kumagai in [2] presented an implementation of an human-inspired handover controller on a robot with compliant under-actuated hands. Concerning the last phase, Strabala in [14] stated that after transferring the entire object load, often the receiver will retract, indirectly signalling the giver that the handover is complete.

3. Handover Algorithm Formulation

The formulation of a successful, fluent and dynamical handover requires the integration of multiple states in each handover phase that together allow a robot to perform the task. The development process of such states is done by formulating a FSM.

3.1. Robot-to-Human Handover

A robot-to-human object handover task aims to achieve an object transfer from a robot to a human where the robot acts as the giver and the human as the receiver. In this manner, a sequence of states and transitions of the FSM proposed were selected as Figure 1 displays in blue. Initially and assuming that the intention to perform a handover has already been established, the first state involves the opening of the gripper, followed by the movement to the object location which is assumed to be known by the robot. Upon arrival, the object must be grasped. It is important to refer that no specific grasping algorithm was designed given that the object grasping field is considered out of the current research goals scope. The next states involves the robot's movement into the handover pre-assigned location. Moreover, the robot should approach the user from the front as this angle provides him/her the most visibility of the robot's motion [10]. Furthermore, the robot's arm should be extended [1]. With the aim of delivering the object in a dynamic and fluent manner, an impedance control-based approach must be activated. This approach implements a dynamic response between the environment acting on the robot's manipulator structure and its motion. Due to the extensive control formulation, this module is further analysed in section 3.3. The impedance control (IC) activation is followed by the state regarding the user signaling in which the robot should communicate to the user that it is ready to deliver the object [14]. Another relevant stage of the transfer phase is the robot's decision concerning the appropriate instance of releasing the object. Following the work developed by Edsinger in [3], the robot's end-effector velocity was monitored. In this manner, if the end-effector velocity is higher then the defined threshold and the robot is grasping the object, the user's receiving intention is detected and the robot will open the gripper. The

retraction phase is the last phase of the handover sequence. If the object has been delivered, the robot must switch off the formulated impedance control and move away from the handover location.

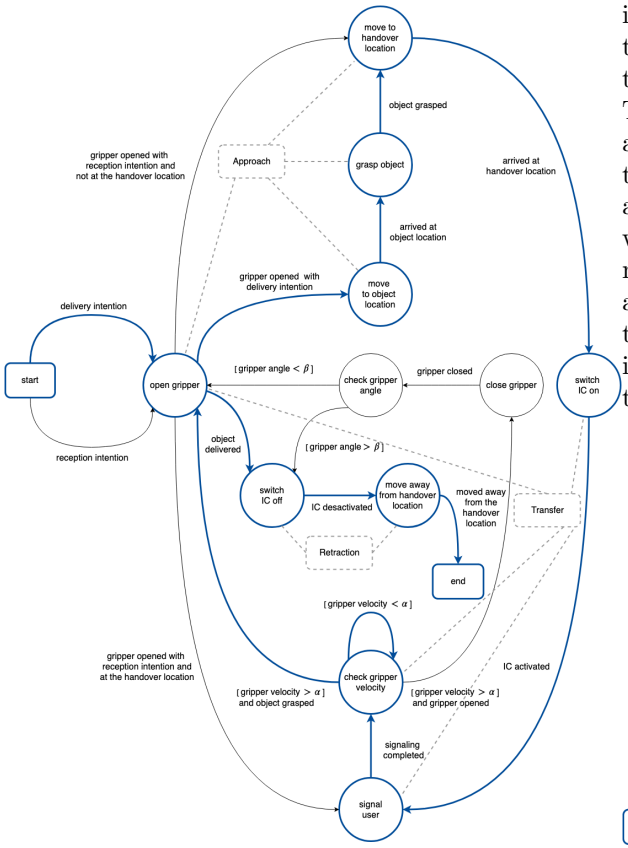

Figure 1: State-machine based algorithm sequence, in blue, regarding a robot-to-human handover. The three phases on the handover are also presented.

3.2. **Human-to-Robot Handover**

The most commonly implemented handover tasks between humans and a robots rely on the robot as a giver and the user as the receiver. Nonetheless, several tasks also require the other way around: human-to-robot object handover. In this handover task, the robot is the receiver and the human performs the giver role. A sequence of transitions and states of the proposed FSM describes a human-to-robot handover and it is presented in Figure 2, in blue. The approach phase is initiated without the object and it is assumed that the robot already acknowledge the intention of receiving an object. As in the previous task, the robot's arm should be extended in the approach phase [1]. Furthermore, the opened gripper during the approach stage emphasis that intention. Upon arrival to the handover location, the same impedance control approach used on the robot-to-human handover task must be activated and the robot must signal the user. Furthermore, the robot must detect that the object has been placed in its end-effector. The work developed by Edsinger in [3] was again taken into consideration. The main difference between the previous task is the value of velocity threshold, α, as this must remain dependent of the robotic behavior implemented and must be once again tuned given the different interaction. Upon closing its gripper, the robot must verify the object reception success. This can be done by checking the resulting grasp aperture: if it is positive and above a threshold, β, then the gripper is assumed to be wrapped around an object and the retraction phase initiates, otherwise the robot must re-open the gripper and signal the user, showing the acknowledgement of the a failed transfer. Lastly, in the retraction phase, the impedance control must be switched off and, implicitly, a mobility controller switch on, allowing the robot to move away from the handover location.

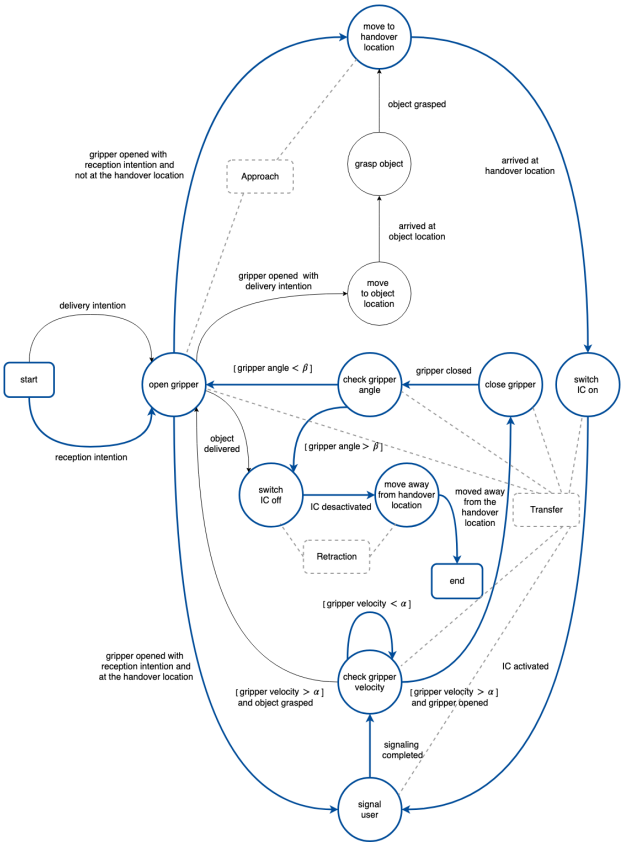

Figure 2: State-machine based algorithm sequence, in blue, regarding a human-to-robot handover. The three phases on the handover are also presented.

3.3. **Impedance Control**

A fluent and dynamic human-robot handover may be achieved due to the robot's adaptability to the task conditions, environmental constraints and perturbations instead of simply controlling its position, in which the robot is seen as an isolated system. As a result, impedance control was selected as the

controlling approach for the transfer phase of the proposed FSM-based handover algorithm. This section aims to formulate an impedance controller that generates a dynamical relationship between a free-flyer robot manipulator and external forces acting on it. This formulation is adapted to this dissertation goals from the research developed by Lippiello and Ruggiero in [13].

3.3.1 Kinematic Model

It is relevant to refer that the derivation is independent of the robot's base configuration. Furthermore, it also does not depend on the arm placement choice as, depending on the particular vehicle configuration, the best mounting of the manipulator that allows a stable behavior will be considered. Additionally, the manipulator consists of n rigid links connected by joints q_l, with $l = 1, 2, 3, ..., n$. At the end of the last link, the one not connected to the vehicle, is a gripper, e.g., end-effector. A schematic representation of free-flying robot and a manipulator is presented in Figure 3 as well as the reference frames considered.

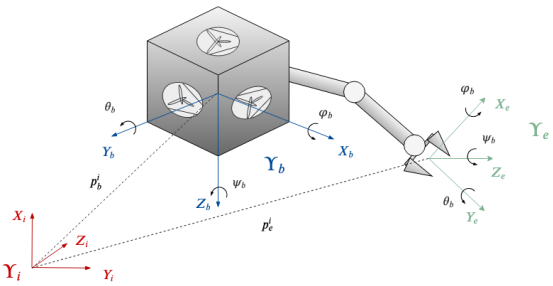

Figure 3: Schematic representation of a generalized free-flyer robot equipped with a manipulator and respective reference frames.

The inertial frame is denoted by Υ_i, the body-fixed reference frame placed at the spacecraft center of mass by Υ_b and the end-effector coordinates attached to the interaction point of the manipulator by Υ_e. Furthermore, the absolute position of Υ_b with respect to Υ_i is described as $p_b^i = [x_b \; y_b \; z_b]^T$ and the system attitude is expressed in roll-pitch-yaw Euler angles being denoted by $\phi_b^i = [\varphi_b \; \theta_b \; \psi_b]^T$. Additionally, the absolute transitional velocity of Υ_b is represented by $\dot{p}_b^i$ and $\dot{p}_b^b$, with respect to Υ_i and to Υ_b, respectively. Regarding the absolute rotational velocity, ω_b^i refers to the absolute rotational velocity of the vehicle and ω_b^b denotes the absolute rotational velocity with respect to Υ_b. If the rotation matrix of frame Υ_b with respect to frame Υ_i is defined by R_b^i, the spacecraft linear velocity representation in Υ_b coordinates is transformed to its representation in Υ_i coordinates from:

$$\dot{p}_b^i = R_b^i \, \dot{p}_b^b \tag{1}$$

Moreover, if the transformation matrix between the time derivative of ϕ_b^i and ω_b^i is defined by N_b^i, the transformation of the UAV absolute rotational velocity is obtained as:

$$\omega_b^i = N_b^i \, \dot{\phi}_b^i \tag{2}$$

From (1) and (2) holds:

$$\omega_b^b = (R_b^i)^T \, \omega_b^i = (R_b^i)^T \, N_b^i \, \dot{\phi}_b^i = Q_b^i \, \dot{\phi}_b^i \tag{3}$$

with $Q_b^i = (R_b^i)^T \, N_b^i$ being the mapping of the time derivative of ϕ_b^i into the body absolute rotational velocity with respect to Υ_b. The transformation equations (1)-(3) are valid as long as the matrices R_b^i, N_b^i, and Q_b^i are non-singular. Furthermore, direct kinematics of the spacecraft are defined by the following transformation matrix:

$$K_b^i(p_b^i, \phi_b^i) = \begin{bmatrix} R_b^i & p_b^i \\ 0_{1\times 3} & 1 \end{bmatrix} \tag{4}$$

where, $0_{1\times 3}$ is a (1×3) vector composed only by zeros. Furthermore, direct kinematics of the manipulator with respect to Υ_b are expressed as:

$$K_e^b(q) = \begin{bmatrix} R_e^b(q) & p_e^b(q) \\ 0_{1\times 3} & 1 \end{bmatrix} \tag{5}$$

with q describing the $(n \times 1)$ vector of the robot manipulator joints variables, R_e^b the rotation matrix between Υ_e and Υ_b and $p_e^b = [x_e^b \; y_e^b \; z_e^b]^T$ the position of the end-effector with respect to Υ_b. Combining (4) and (5):

$$K_e^i(\xi) = K_b^i \, K_e^b \tag{6}$$

where $\xi = [{p_b^i}^T \; {\phi_b^i}^T \; q_1 \; ... \; q_n]^T$ is the $((6+n) \times 1)$ generalized vector of the system joints variables. Moreover, the end-effector absolute position with respect to the inertial frame is defined as $x = [p_e^i \; \phi_e^i]$ where $p_e^i = [x_e \; y_e \; z_e]^T$ and the manipulator's attitude is also expressed in roll-pitch-yaw Euler angles being denoted by $\phi_e^i = [\varphi_e \; \theta_e \; \psi_e]^T$ with respect to Υ_i. The vector of absolute generalized velocity of the manipulator's end-effector can consequently be expressed as $\dot{x} = [\dot{p}_e^i \; \dot{\phi}_e^i]$. Furthermore, the same consideration as Equation (2) holds for the end-effector with:

$$\omega_e^i = N_e^i \, \dot{\phi}_e^i \tag{7}$$

The transformation between $\dot{x}$ and the time derivative of the system generalized joints variables can be written as:

$$\dot{x} = J \, \dot{\xi} \tag{8}$$

where J is the so called Jacobian $(6\times(6+n))$ matrix of the system. Moreover, time deriving equation (8) yields:

$$\ddot{x} = J\ \ddot{\xi} + \dot{J}\ \dot{\xi} \tag{9}$$

Furthermore, the linear and angular velocity of the center of mass of the link i with respect to Υ_b, $\dot{p}^b_{bl_i}$ and $\omega^b_{bl_i}$, respectively, can be expressed by:

$$\dot{p}^b_{bl_i} = J^{l_i}_t\ \dot{q} \tag{10a}$$

$$\omega^b_{bl_i} = J^{l_i}_r\ \dot{q} \tag{10b}$$

Lastly, the position of the center of mass of the link i with respect to Υ_i is described as:

$$p^i_{l_i} = p^i_b + R^i_b\ p^b_{bl_i} \tag{11}$$

3.3.2 Dynamic Model

The controller designed should consider the dynamics of the free-flyer as the manipulator aerial base and of the manipulator, simultaneously. Accordingly, using a *Euler-Lagrange* formulation and kinematics relations derived in previous section, the dynamics of the system in the generalized joint space, ξ, is obtained.

According to the *Euler-Lagrange* formulation, a system mechanical structure can be described by the sum of its total kinetic energy, T, and potential energy, U. In a microgravity environment, the potential energy is considered to be identically zero as $g \approx 0$. Therefore, the total energy, L, of the proposed system is:

$$L = T \tag{12}$$

The Lagrange equations can be defined as:

$$\frac{d}{dt}\frac{\partial L}{\partial \dot{\xi}_i} - \frac{\partial L}{\partial \xi_i} = u_i \tag{13}$$

with i describing the i-th generalized coordinate of ξ and assuming values of $i = 1, ..., ((6 + n))$. The i-th generalized force is represented as u_i. The total kinetic energy of the system being studied is composed by the energy contributions concerning the motion of the spacecraft, T_b and the energy associated with motion of each link of the manipulator, T_{l_i}, as express in Equation (14).

$$T = T_b + \sum_{i=1}^{n} T_{l_i} \tag{14}$$

The aerial vehicle kinetic energy contribution is expressed by:

$$T_b = \frac{1}{2}\ m_b\ \dot{p}^{i\,T}_b\ \dot{p}^i_b + \frac{1}{2}\ \dot{\phi}^{i\ T}_b\ Q^{i\ T}_b\ H_b\ Q^i_b\ \dot{\phi}^i_b \tag{15}$$

with H_b and m_b representing the inertia and mass matrix of the free-flyer, respectively. Having into account that the $R^b_{l_i}$ is the rotation matrix between the center-of-mass of the i-th manipulator link and Υ_b, m_{l_i} is the mass and H_{l_i} is the inertia matrix of the i-th link, the kinematic energy of the manipulator is then described as:

$$T_{l_i} = \frac{1}{2}\ m_b\ \dot{p}^{i\ T}_{l_i}\ \dot{p}^i_{l_i} + \frac{1}{2}\ \omega^{i\ T}_{l_i}\ R^i_b\ R^b_{l_i}\ H_{l_i}\ R^{l_i}_b\ R^{i\,T}_b\ \omega^i_{l_i} \tag{16}$$

Knowing (3), (10a), (10b), (15) and (16) the total kinetic energy is:

$$L = T = \frac{1}{2}\ \dot{\xi}^T\ B\ \dot{\xi} \tag{17}$$

with B being an $((6 + n) \times (6 + n))$ symmetric and positive inertia matrix. Lastly, computing the Lagrange equation (13), the dynamics of the system in the generalized joint space are given by:

$$B(\xi)\ \ddot{\xi} + C(\xi, \dot{\xi})\ \dot{\xi} = u + u_{ext} \tag{18}$$

where u describes the generalized input forces vector $((6 + n) \times 1)$ and u_{ext} represents the external generalized forces vector at a joint level, $((6+n)\times1)$. Furthermore, C is an $((6+n)\times(6+n))$ matrix that encompasses the Coriolis and centrifugal terms and whose generic element is c_{ij}:

$$c_{ij} = \sum_{k=1}^{(6+n)} \frac{1}{2}\ \left(\frac{\partial b_{ij}}{\partial \xi_k} + \frac{\partial b_{ik}}{\partial \xi_j} + \frac{\partial b_{jk}}{\partial \xi_i}\right) \dot{\xi}_k \tag{19}$$

with b_{ij} representing the generic element of $B(\xi)$, $i, j = 1, ..., (6 + n)$.

3.3.3 Control Law

Given that the kinematics and dynamics model of the system were already described, this section uses those formulations to design a control law that agrees with an impedance dynamical model.

Let $\ddot{x}_d$, $\dot{x}_d$ and x_d be the end-effector desired *rest* acceleration, velocity and position, respectively, and the actual position error as $\tilde{x} = x_d - x$. Moreover, during the transfer phase on the the handover tasks formulated it is assumed that $\ddot{x}_d = 0$ and $\dot{x}_d = 0$. Given these considerations, a suitable law control can be designed:

$$u = J^T\ (-k_B\ \dot{x} + k_D\ \tilde{x}) \tag{20}$$

With k_D and k_B representing the $((6+n)\times(6+n))$ symmetric and positive definite matrices of the chosen stiffness and damping, respectively. It is important to refer that this matrices can be tuned to the desired system's behavior. Finally, substituting (20) into (18) and considering (8) and (9), the joint space dynamics can be expressed in terms of the manipulator's end-effector configuration, x, in the inertial Cartesian coordinates representing an

impedance dynamic model as presented in Equation (21).

$$B_x\ \ddot{x} + (C_x + k_B)\ \dot{x} - k_D\ \tilde{x} = f_{ext} \tag{21}$$

with f_{ext} representing the vector $((6+n)\times 1)$ of the external generalized forces at the Cartesian coordinate level and B_x and C_x describing the inertia and Coriolis matrices with respect to the x variable:

$$B_x = J(\xi)^{-T}\ B(\xi)\ J(\xi)^{-1} \tag{22a}$$

$$C_x = J(\xi)^{-T}\ (C(\xi,\dot{\xi}) - B(\xi)\ J(\xi)^{-1}\ \dot{J}(\xi))\ J(\xi)^{-1} \tag{22b}$$

4. Implementation and Results

The current section concerns about the algorithm implementation and validation on a simulator. Furthermore, an implementation of a human interaction interface with the system is also described and validated.

4.1. Formulated Algorithm Implementation

4.1.1 Astrobee Robot Software and Handover ROS Node

Given the current collaboration between NASA and ISR and the availability of an open-source Astrobee software platform designed to conduct research [4], this free-flyer robot simulator was used as an implementation platform to showcase and verify the proposed handover algorithm. The software architecture is composed by 46 ROS nodelets. Moreover, the nodelets are grouped into modules running across three main computers: the Low-Level (LLP), Mid-Level (MLP) and High-Level Processor (HLP). Furthermore, the implementation of the handover algorithm requires the integration of multiple functionalities in each phase that together allow a robot to perform the task. In this manner, a ROS node was developed and connects to the several components of the LLP and MLP of the Astrobee Software and includes multiple modules that are used on the algorithm implementation. The proposed algorithm node was implement using Python 3.0, Ubuntu 16.04 LTS and ROS Kinetic. Regarding the impedance control module, it is important to refer that although an impedance control formulation for a free-flyer robot equipped with a manipulator was described on section 3.3, the Astrobee's simulator presented considerably small tolerances for the joints state goals. Thus, it not allows the movement of the arm links for small controlled angles and the joint variables are assumed to be fixed for this implementation. In this manner:

$$\dot{\xi} = [\dot{p}_b^{i\,T}\ \dot{\phi}_b^{i\,T}\ 0\ ...\ 0]^T \tag{23}$$

Consequently, the input vector of the manipulator actuation torques is irrelevant and the input vector of forces, f, is composed by the free-flyer base actuator force vector, F (3×1), and torque vector, M (3×1):

$$f = \begin{bmatrix} F^T \\ M^T \end{bmatrix} \tag{24}$$

Furthermore, considering the configuration of the Astrobee, the vector u has the following expression:

$$u = \begin{bmatrix} R_b^i \\ Q_b^{i\,T} \end{bmatrix} f \tag{25}$$

Moreover, two types of impedance behaviors were implemented: rigid and compliant. This behaviors can be defined by tuning the values of the matrices in Equation (20). The tuned values for the matrices are presented in Table 1 with $m_{3\times 3}$ being a (3×3) matrix representing the mass of the system and its inertial vales being presented by $H_{3\times 3}$.

		Rigid behavior	Compliant behavior
Linear Component	k_D	$7\mathrm{m}_{3\times 3}$	$0.7\mathrm{m}_{3\times 3}$
	k_B	$15\mathrm{I}_{3\times 3}$	$5\mathrm{I}_{3\times 3}$
Rotational component	k_D	$70\mathrm{H}_{3\times 3}$	$7\mathrm{H}_{3\times 3}$
	k_B	$5\mathrm{I}_{3\times 3}$	$\mathrm{I}_{3\times 3}$

Table 1: Matrices values in Equation (20) tuned accordingly to the desired Astrobee behavior: rigid or compliant.

4.1.2 Impedance Control Validation

In order to obtain the formulated impedance controller validation during interaction, several generalized external forces, f_{ext}, were applied to the robot's end-effector, for both behavior study cases: rigid and compliant. Furthermore, with the aim of validating the dynamic impedance model proposed (Equation (21)), the expected values of the end-effector position and orientation error, $\tilde{x}'$, were calculated from Equation (21) given the end-effector simulated acceleration, $\ddot{x}$, the end-effector simulated velocity, $\dot{x}$, the B_x, C_x, K_D and K_B matrices and the f_{ext}, as following:

$$\tilde{x}' = [B_x\ \ddot{x} + (C_x + k_B)\ \dot{x}\ - f_{ext}]\ /\ k_D \tag{26}$$

The calculated end-effector position and orientation error, $\tilde{x}'$, as well as the actual simulated end-effector position and orientation error, $\tilde{x}$, are presented each axis in Figure 4 for the rigid behavior and for the compliant behavior case. Additionally, the external generalized forces generated for each simulation are represented. For all tests performed, the end-effector initial state and the end-effector desired state were defined as $x_{initial} = [0, -0.07, 0, 0, 0, 0]$ and $x_d = x_{initial}$, respectively.

Analysing the presented figures, several conclusions can be drawn. The first one concerns the

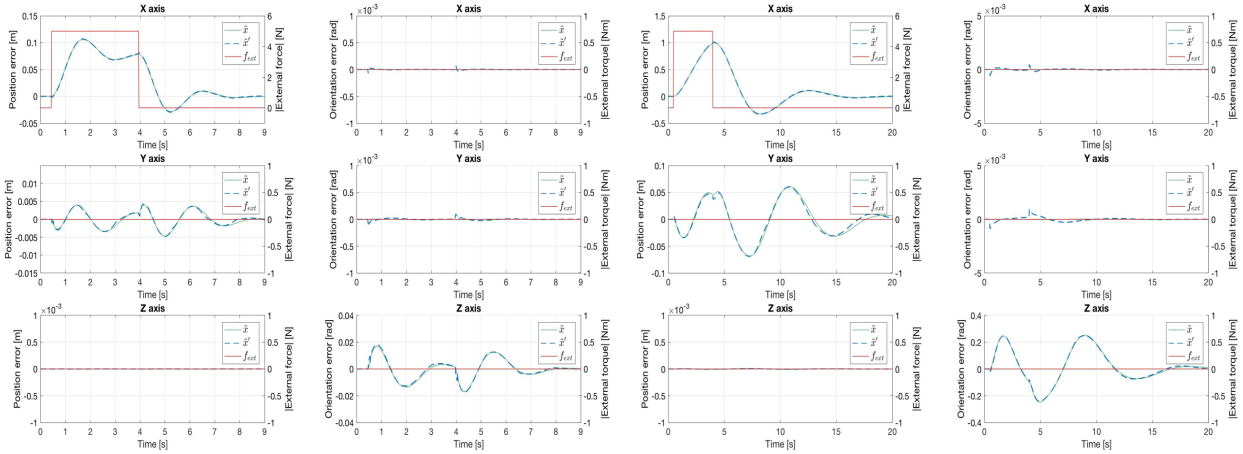

Figure 4: Actual and calculated (from impedance model) end-effector position and orientation error, with a rigid behavior (6 figures on the left) and compliant behavior (6 figures on the right). A $5N$ force was applied on the X axis.

clear motion distinction between the two behaviors: a higher stiffness value in Equation (21) generates a rigid behavior where the end-effector tends to reach the desired state with a lower position/orientation error and a lower stiffness value generates robot's motion passively to the external perturbation, diverging more from the desired state. Furthermore, the robot not only reaches for desired/rest state for both behaviors while an external force acts on the end-effector, but also in the absence of external perturbations. Lastly, the end-effector behaves accordingly to desired impedance model expressed by Equation (21). This can be concluded due to the overlap of the actual simulated end-effector error motion, $\tilde{x}$, and the calculated end-effector error motion from the impedance model, $\tilde{x}'$.

4.2. Human Interaction Implementation

The algorithm proposed assumes that two agents are involved in the handover: a robot and a human. Thus, the current section aims to describe the user interaction interface implementation and validation.

4.2.1 Simulated Hand Model Control through a Leap Motion Device

The main requirement concerning the simulated hand model relayed on its the ability to perform grasping motions similar to the human hand. To produce these motions, the hand should have five fingers. Therefore, the iCub hand was selected and integrated into the Gazebo 7.0 simulation. With the aim of obtaining the control values for the simulated hand and fingers from a real user hand, a Leap Motion device was integrated on the interface. This device is a tracking device which main purpose is the tracking of human hand and fingers. To achieve the hand data, the Leap Motion SDK (Software Development Kit) that interfaces the device with Ubuntu 16.04 was used and a ROS node that fetched the fingers position and the hand position/attitude from the SDK and published it as ROS topic to the control topics was integrated.

4.2.2 Results

With the aim of validating the previous described implementation, several tests were carried out with the simulated hand model and the Leap Motion device where hand translation/rotation motions and finger displacement were evaluated. Figure 5 displays the pitch test with the tracked user hand orientation, in blue, and the simulated hand model orientation, in green, respectively.

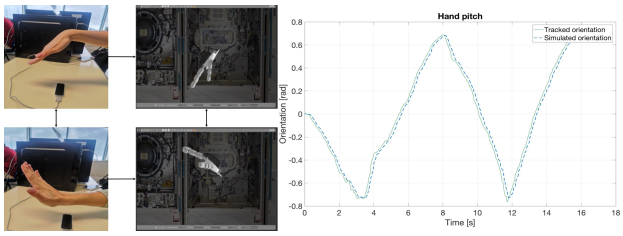

Figure 5: The four figures on the left represent the user hand pitch and the respective simulated hand motion, while the plot on the right encompasses the pitch data.

As is possible to observe from test results, the simulated hand motion is successfully controller through the Leap Motion device.

4.3. **Handover Algorithm Results**

With the aim of validating the proposed handover algorithm, a robot-to-human and human-to-robot handover task were performed with a robot rigid and compliant behavior and using the user interaction interface developed. Figure 6 displays the user hand, the Leap Motion device and the simulation environment.

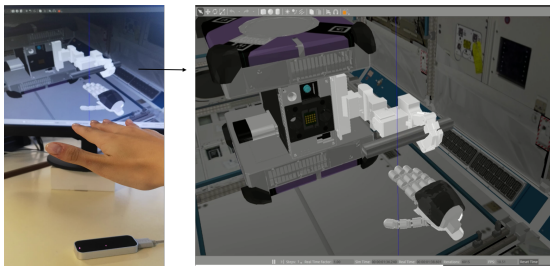

Figure 6: Representation of the user hand controlled via Leap Motion and the simulation environment.

4.3.1 Robot-to-Human

The first validation tests were performed concerning the robot-to-human handover where the robot acts as the giver and the user as the receiver. The motion results are shown in Figure 7 and 8 for the rigid and compliant behavior, respectively. Additionally, the gripper angle and linear velocity are also represented. The handover sequence is well perceived by analysing the referred figures. As formulated, the robot initiates the handover with a closed gripper and without the object. It then opens the gripper, gets closer to the object and grabs it 13 seconds after initiating the task. Following, the robot moves to the handover location ($x = 0,\ y = -0.07,\ z = 0$) with 0 orientation in all axis. After activating the IC (Impedance Control), the robot is ready to deliver the object and the Transfer phase initiates in which the robot signals the user and waits for the gripper velocity threshold. When this occurs, the robot opens its gripper and the object is transferred to the user. Lastly, both move away from the handover location, during the Retraction phase. Furthermore, it is interesting to scrutinize the Z position representation for the same figures. On the rigid behavior simulation, the gripper moves $0.04m$ when the user interaction is happening, whereby on the compliant case the robot reaches $0.14m$ away from the handover location. Therefore, during the transfer, the gripper motion is in accordance to the impedance control results, given that, for a similar user external interaction, the gripper's movement is minimum for a rigid behavior and it follows the simulated user hand for the compliant case.

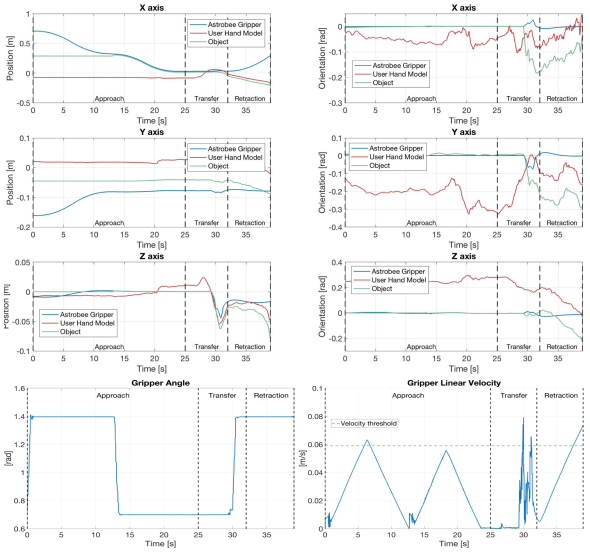

Figure 7: Results of a robot-to-human object handover with a rigid behavior.

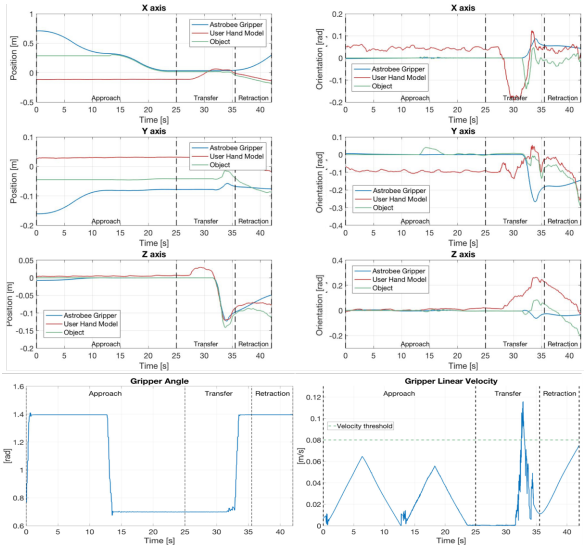

Figure 8: Results of a robot-to-human object handover with a compliant behavior.

4.3.2 Human-to-Robot

The second validation tests were performed concerning the human-to-robot handover where the robot acts as the receiver and the user as the giver. The results are shown in Figure 9 and 10 for the rigid and compliant behavior, respectively. As in the previous task results, the handover sequence is well perceived by analysing the X error position of both figures. In this case, the robot initiates the handover with a closed gripper and without the object as the user is grabbing it. It then opens the gripper and moves to the same handover location (x=0, y=-0.07, z=0) maintaining an open gripper. After activating the IC, the robot is ready to receive

the object and thus, the Transfer phase begins in which the robot signals the user and waits to detect the object placement on its end-effector through the exceed of the gripper velocity threshold. When this occurs, the transfer of the object is performed and the user hand model and the Astrobee move away from the handover position. Moreover, the X error position representation also shows twice the end-effector displacement for the compliant behavior when compared to the rigid behavior during the object's transfer. Thus, as expected, the Astrobee moves more passively to the user interaction on the compliant case.

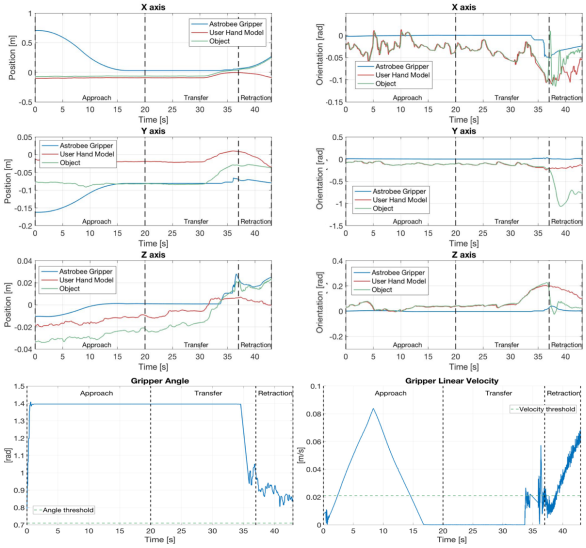

Figure 9: Results of a human-to-robot object handover with a rigid behavior.

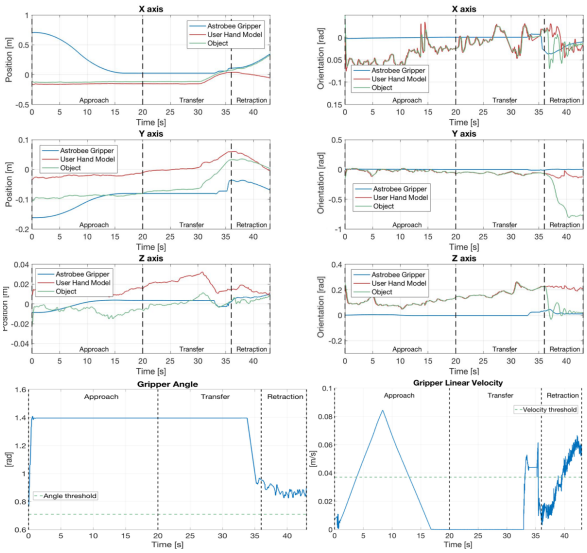

Figure 10: Results of a human-to-robot object handover with a compliant behavior.

5. User Study

The current section aims to describe the systematic user study conducted. Based on the results of Kupcsik's study [7] it is known that for static handover tasks using cartesian compliant control, compliance parameters are less important for success and high stiffness is always preferred and highly rated. Gasparri in [5] shows that when using impedance handover dynamics the optimal manipulator stiffness is high in the case of perfect knowledge of the framework. In this sense, the systematic user study aimed to explore the subjective outcomes effects on the user concerning the implemented robot behaviors. Furthermore, the handover success of the two behaviors was also studied.

Two hypothesis were in advance proposed for the experimental study: **H1** - "The impedance control parameters will affect the participant's perception of the object handover task with high stiffness (rigid behavior) being the most fluent, desirable and cooperative and low stiffness (compliant behavior) the less fluent, desirable and cooperative"; **H2** - "The impedance control parameters will affect the object handover task success with high stiffness (rigid behavior) being the most successful and low stiffness (compliant behavior) the less successful"

Ten people with ages between 21-30 participated in this experiment (6 female and 4 male).

5.0.1 Procedure and Measures

Initially each participant performed different manoeuvres of their choice with the simulated hand for 10 minutes. The second section of the experiment was the handover tasks: robot-human, human-robot handover and a collaborative task that encompassed both handovers. Moreover, the controller parameters conditions were manipulated to achieve rigid robot behavior or compliant robot behavior during each task. These comprised six experimental conditions in total. Therefore, the study involved 12 rounds of interaction for each participant – two for each experimental condition with randomized controlled trials. After each round of interaction, participants filled out a questionnaire giving a score between 1 (fully disagree) and 9 (fully agree) [11] to three statements regarding their perception of the handover in which subjective measures were evaluated. In particular three scales were used — fluency [6] and [8], satisfaction [11] and team work [6]. The statements were the following: **S1** - *The robot contributed for the fluency of the interaction.*; **S2** - *I was satisfied with the interaction.*; **S3** - *The robot was committed to the task.* Additionally, the number of non-successful object handover in the three tasks were registered.

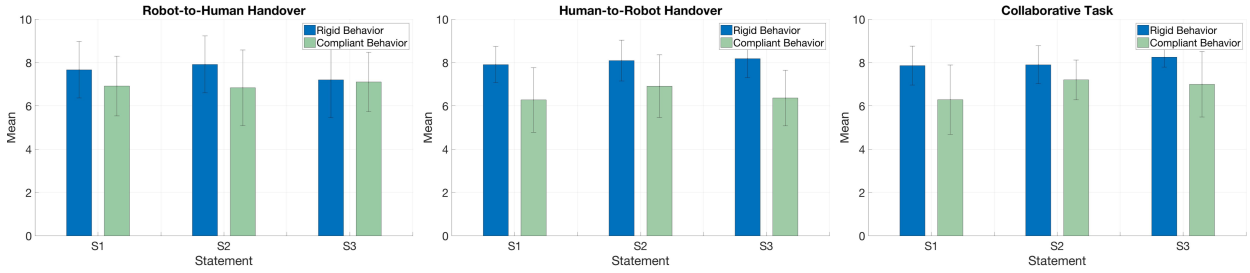

Figure 11: Representation of the mean and standard deviation of the questionnaire's results for the performed tasks.

5.0.2 Results

The questionnaire's results are presented in Figure 11, for the proposed tasks. Additionally, Table 2 displays the total number of failed transfers for each task.

		Rigid Behavior	Compliant Behavior
Task	Robot-to-Human Handover	3	3
	Human-to-Robot Handover	0	2
	Collaborative	2	3

Table 2: Total number of failed handovers on the three performed tasks.

Concerning the user's responses to the proposed statements, the results indicate that in a robot-to-human handover scenario users perceived higher fluency for a rigid behavior (p-value = 0.1195, $\alpha = 0.05$) and were more satisfied with the interaction also for the rigid behavior (p-value = 0.0589, $\alpha = 0.05$). Moreover, no substantial difference between both behaviors was felt regarding the robot commitment to the task (p-value = 0.8880, $\alpha = 0.05$) and thus concerning the cooperation perceived. Additionally, results shows higher distinction between the answers regarding the two behaviors in the human-to-robot handover scenario, as users perceived more fluency, satisfaction and cooperation for a rigid behavior (p-value of 0.0132, 0.0401 and 0.0057, respectively and with $\alpha = 0.05$). As expected, for the collaborative task, the results were also higher for the rigid behavior concerning S1, S2 and S3 (p-value of 0.0375, 0.0445, 0.0492, respectively and with $\alpha = 0.05$). Lastly, more total successful handovers were performed for the rigid behavior. Summarizing, the results indicate that H1 was verified for the first two factors and the handover success data supported H2 for the human-to-robot object handover and collaborative task.

6. Conclusions and Future Work

This dissertation formulated and validated an algorithm that enabled a free-flyer robot to perform an object handover with a human in a microgravity environment on a dynamic, fluent and successful manner with resource to a FSM and impedance control. Furthermore, two impedance robot behaviors were studied: rigid and compliant. As the results portrait, the robot followed the desired state and behaved accordingly to the derived impedance model for both cases. Additionally, the formulated algorithm was successfully validated for both tasks, robot-to-human handover and human-to-robot handover, with both robot behaviors, rigid and compliant. Lastly, an accurate user interaction interface was developed and a systematic user study was conducted. Results showed that the rigid behavior was overall more preferable and registered higher transfer success during the proposed tasks.

Future work may address a possible grasping algorithm, a non-fixed joint scenario and the algorithm implementation on two robots for handovers tasks with objects of higher dimensions.

References

[1] M. Cakmak, S. S. Srinivasa, M. K. Lee, S. Kiesler, and J. Forlizzi. Using spatial and temporal contrast for fluent robot-human handovers. *International Conference on Human-Robot Interaction (HRI)*, pages 489–496, 2011.

[2] W. P. Chan, I. Kumagai, S. Nozawa, Y. Kakiuchi, K. Okada, and M. Inaba. Implementation of a robot-human object handover controller on a compliant underactuated hand using joint position error measurements for grip force and load force estimations. *IEEE International Conference on Robotics and Automation (ICRA)*, 2014.

[3] A. Edsinger and C. C. Kemp. Human-robot interaction for cooperative manipulation: Handing objects to one another. *The 16th IEEE International Symposium on Robot and Human Interactive Communication (RO-MAN)*, 2007.

[4] L. Fluckiger, K. Browne, B. Coltin, J. Fusco, T. Morse, and A. Symington. Astrobee robot software: Enabling mobile autonomy on the iss. *Proceedings of the International Symposium on Artificial Intelligence, Robotics and Automation in Space (i-SAIRAS)*, 2018.

[5] G. M. Gasparri, F. Fabiani, M. Garabini, L. Pallottino, G. G. M. Catalano, R. Persichin, and A. Bicchi. Robust optimization of system compliance for physical interaction in uncertain scenarios. *IEEE-RAS 16th International Conference on Humanoid Robots*, 2016.

[6] G. Hoffman. Evaluating fluency in human-robot collaboration. *IEEE Transactions on Human-Machine Systems*, 49(3):209–218, June 2019.

[7] D. K. Hsu and W. S. Lee. Learning dynamic robot-to-human object handover from human feedback. *Springer Proceedings in Advanced Robotics Research*, page 161–176, 2017.

[8] C. M. Huang, M. Cakmak, and B. Mutlu. Adaptive coordination strategies for human-robot handovers. *Robotics: Science and Systems XI (RSS)*, 2015.

[9] V. M. J. Aleotti and S. Caselli. Comfortable robot to human object hand-over. *Robot and Human Interactive Communication (RO-MAN)*, pages 771–776, 2012.

[10] K. Koay, E. Sisbot, and D. Syrdal. Exploratory studies of a robot approaching a person in the context of handing over an object. *AAAI Spring Symposium: Multidisciplinary Collaboration for Socially Assistive Robotics*, pages 18–24, 2007.

[11] M. Koene, S. Endo, A. Remazeilles, M. Prada, and A. M. Wing. Experimental testing of the coglaboration prototype system for fluent human-robot object handover interactions. *The 23rd IEEE International Symposium on Robot and Human Interactive Communication (RO-MAN)*, 2014.

[12] A. Kupcsik, D. Hsu, and W. S. Lee. Learning dynamic robot-to-human object handover from human feedback. *Springer Proceedings in Advanced Robotics Robotics Research*, pages 161–176, 2017.

[13] V. Lippiello and F. Ruggiero. Cartesian impedance control of a uav with a robotic arm. *IFAC Proceedings Volumes*, 45(22):704–709, 2012.

[14] K. W. Strabala, M. K. Lee, J. L. F. A. D. Dragan, S. Srinivasa, M. Cakmak, and V. Micelli. Towards seamless human-robot handovers. *Human–robot interaction*, 2(1):112–132, 2013.